Validating GEOV1 Fractional Vegetation Cover Derived From Coarse-Resolution Remote Sensing Images Over Croplands

Xihan Mu, Shuai Huang, Huazhong Ren, Guangjian Yan, Wanjuan Song, and Gaiyan Ruan

***Abstract*—Fractional vegetation cover (FVC) is one of the most important criteria for surface vegetation status. This criterion corresponds to the complement of gap fraction unity at the nadir direction and accounts for the amount of horizontal vegetation distribution. This study aims to directly validate the accuracy of FVC products over crops at coarse resolutions (1 km) by employing field measurements and high-resolution data. The study area was within an oasis in the Heihe Basin, Northwest China, where the Heihe Watershed Allied Telemetry Experimental Research was conducted. Reference FVC was generated through upscaling, which fitted field-measured data with spaceborne and airborne data to retrieve high-resolution FVC, and then high-resolution FVC was aggregated with a coarse scale. The fraction of green vegetation cover product (i.e., GEOV1 FVC) of SPOT/VEGETATION data taken during the GEOLAND2 project was compared with reference data. GEOV1 FVC was generally overestimated for crops in the study area compared with our estimates. Reference FVC exhibits a systematic uncertainty, and GEOV1 can overestimate FVC by up to 0.20. This finding indicates the necessity of reanalyzing and improving GEOV1 FVC over croplands.**

***Index Terms*—Coarse resolution, fractional vegetation cover, product validation, SPOT/VEGETATION.**

I. Introduction

THE COMMITTEE on Earth Observation Satellites considers such satellites and complementary *in situ* networks as vital to effective monitoring and prediction of changes in climate systems on Earth [1]. Coarse-resolution satellite data exhibit advantages at the global scale. These data are easily obtained and widely used to estimate research and application parameters. Spatial resolutions between 250 m and 5 km are defined as coarse resolutions [2]. Coarse-resolution data have high-temporal resolutions and are commonly applied to long-term global observations of land surfaces, biospheres, atmospheres, and oceans. Validating coarse-resolution products is critical but problematic. The feasibility and accuracy of remote sensing products must be initially verified before data can be applied. At the minimum, the extent of data quality must be determined. Direct validation using *in situ* data is spatially insufficient to cover an area with one or more coarse pixels because of field measurement limitations [3]. Large-scale campaigns and experiments, such as BigFoot [4], SAFARI2000 [5], Validation of Land European Remote Sensing Instruments (VALERI) [6], and Watershed Allied Telemetry Experimental Research (WATER) [7], have been implemented. Subpixel variability should be considered in estimating vegetation parameters at a coarse resolution because of the large scale of pixels [8]. Morisette *et al*. [9] proposed a bottom-up approach to validate coarse-resolution products using elementary sampling units (ESUs), transfer functions, and high-resolution images. Several experiments have applied upscaling methods to convert local biophysical measurements into high-resolution maps, and subsequently, into coarse-resolution products [6], [10]. VALERI adopted empirical transfer functions and high-resolution images derived from remote sensing. This campaign applied a pragmatic approach in using high-resolution data with minimum field calibrations for mapping vegetation parameters [11]. In this study, we used fractional vegetation cover (FVC) to validate a coarse-resolution product via an upscaling strategy.

FVC is a structural vegetation parameter that significantly influences analysis and evaluation of the ecological environment, ecological balance, and development trend. FVC estimation generally uses field measurements and remote sensing techniques. Digital photography is the most common method to obtain FVC field measurements [12]–[14]. Regression methods (e.g., vegetation index) and machine-learning methods are frequently employed to derive FVC products from remote sensing data at the global scale. Commonly used methods for FVC extraction and current FVC products are summarized in [15]. Such products, which are mainly derived from Polarization and Directionality of the Earth's Reflectances (ADEOS/POLDER), Medium Resolution Imaging Spectrometer (ENVISAT/MERIS), (SPOT/VEGETATION), and Spinning-Enhanced Visible and Infrared Imager (MSG/SEVIRI) sensors, are also listed in the validation report of Land Surface Analysis Vegetation Products (2008; http://landsaf.meteo.pt/GetDocument.do?id=301).

Manuscript received October 15, 2013; revised July 09, 2014; accepted July 13, 2014. Date of publication August 14, 2014; date of current version February 09, 2015. This work was supported in part by the National High Technology Research and Development Program of China under Grant 2012AA12A304, in part by the NSFC under Grant 91125004 and Grant 41101309, in part by the Fundamental Research Funds for the Central Universities under Grant 104-105578GK, and in part by the Special Foundation for Free Exploration of State Laboratory of Remote Sensing Science (13ZY-10).

X. Mu, S. Huang, G. Yan, W. Song, and G. Ruan are with the State Key Laboratory of Remote Sensing Science, Research Center for Remote Sensing and GIS, and School of Geography, Beijing Normal University, Beijing 100875, China (e-mail: muxihan@bnu.edu.cn; gjyan@bnu.edu.cn).

H. Ren is with the Institute of Remote Sensing and Geographic Information System, Peking University, Beijing 100871, China.

Color versions of one or more of the figures in this paper are available online at http://ieeexplore.ieee.org.

Digital Object Identifier 10.1109/JSTARS.2014.2342257

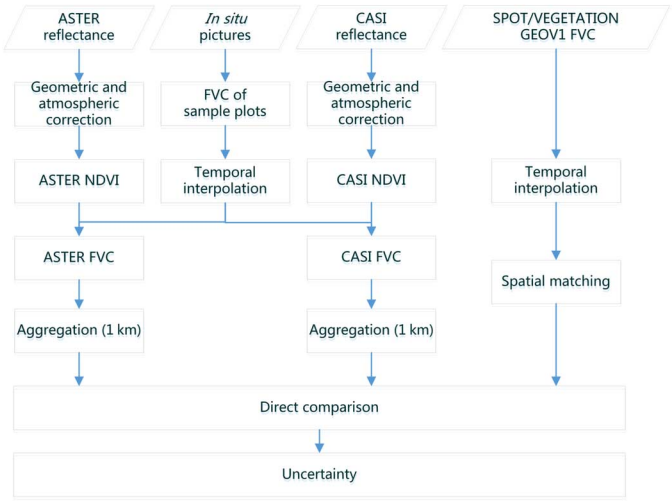

Fig. 1. Data processing and validation strategy.

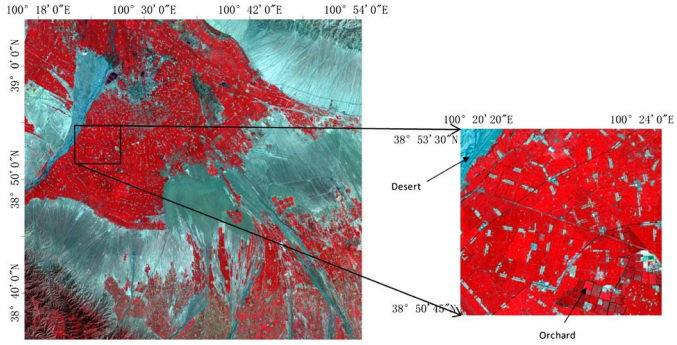

Fig. 2. False-color picture derived from ASTER reflectance on May 30, 2012, which illustrates the study area at the right frame. The red part represents vegetation (i.e., cornfields), whereas the green and blue parts represent desert and artificial areas, respectively.

Carbon Cycle and Change in Land Observational Products from an Ensemble of Satellites (CYCLOPES) [16], GEOV1 [17], and POLDER FVC products are derived from SPOT/VEGETATION and ADEOS/POLDER data that provide global FVCs. GEOV1 FVC is a product based on a CYCLOPES FVC product that corrects underestimation [17].

Although coarse-resolution data have high temporal frequency, vegetation phenology is another issue that affects validation. Fillol *et al*. [18] compared FVCs from Satellite Pour l'Observation de la Terre (SPOT) with those from *in situ* measurements and found that FVC results are related to temporal interpolations. However, interpolation algorithms are difficult to apply in vegetation that exhibits nonlinear and rapid changes.

In 2012, the Heihe Watershed Allied Telemetry Experimental Research (HiWATER) was performed in the Heihe River Basin, China [19] with the aim of improving observation of hydrological processes in arid and semiarid regions. The ground-measured and airborne FVC data employed in this study were acquired during the HiWATER project. The GEOV1 FVC coarse-resolution product (distributed at http://land.copernicus.eu/global/products/fcover) was validated through observations obtained during a crop-growing cycle. GEOV1 FVC was derived from SPOT/VEGETATION sensors with a 10-day temporal sampling and approximately 1 km spatial sampling. The generation of reference data and validation strategies is summarized in Fig. 1. Advanced Spaceborne Thermal Emission and Reflection Radiometer (ASTER) FVC was estimated from ASTER surface reflectance data (ASTER L1B) and field-measured data. Airborne data obtained from the Compact Airborne Imaging Spectrometer (CASI) were processed similarly. GEOV1 FVC was processed by temporal interpolation and compared directly with aggregated FVC throughout the growing season.

II. Study Area and Data Description

A. Study Area

The study area is part of the Heihe River Basin in the arid region of China. The study period was from May to September 2012. The Heihe River is the second longest continental river in China. The HiWATER project chose this area as an experimental watershed for its research plan with the scientific objective of improving the observation of hydrological and ecological processes [19].

The test site is located in an artificial oasis that consists of agricultural land (72%), residential land (24%), and woodland (4%), as shown in Fig. 2. Irrigated and economic crops are planted in the agricultural land. Corn is the dominant vegetation type, and small patches of orchards and land planted with pepper, cauliflower, celery, red bean, and watermelon are also found. A coarse-resolution FVC product was verified using high-resolution remote sensing data. *In situ* data were then prepared to develop a multiscale data set. Observational data included ground-based FVC measurements, radiance images from ASTER and CASI, GEOV1 FVC products, and several ancillary data such as Moderate Resolution Imaging Spectroradiometer (MODIS) aerosol data, aerosol optical thickness measured with a sun photometer, and solar-target observational geometry data.

The hierarchy process for conducting upscaling and accurately estimating FVC includes transfer from *in situ* FVC to FVC derived from ASTER and CASI, and then a consecutive transfer to the coarse-resolution FVC.

B. Ground Measurements of Reference FVC

1) Site Extent and Sampling Strategy: FVC ground measurements were collected via digital photography from May 24 to September 14, 2012. Sampling unit positions were optimized using the mean of surfaces with nonhomogeneity (MSN) [20]. This sampling method considers the autocorrelation and stratified nonhomogeneity of an area through a classification map and other reference data (e.g., a vegetation index map obtained in 2011). MSN ensures reasonable representativeness of a study area with limited sampling units. A total of 22 sampling plots were distributed throughout the area; among these, 16 plots were located in cornfields. The measurement frequency was initially 5 days (before late July) and was increased to 10 days afterward. Ground measurements can be considered as FVC ground truth at the scale of ASTER pixels for upscaling. Artificial cropland is the dominant land cover type in the study area. Agricultural management and

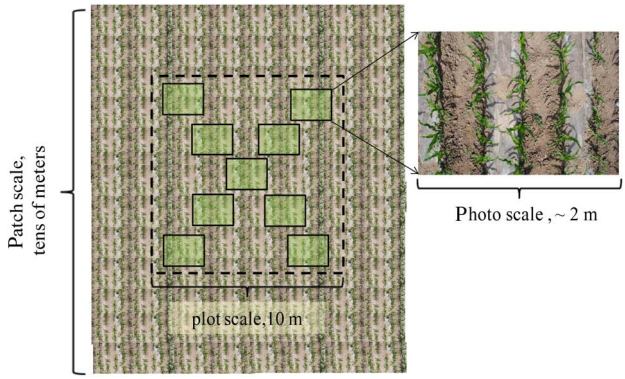

Fig. 3. Schematic of a cropland photograph, which shows the spatial relationships among a cropland patch, a sampling plot, and the photographs taken in a plot.

vegetation growth status are considered to be homogeneous within a cropland patch that typically occupies a rectangular area with a side length of tens of meters. Similar to ESUs [9], our sampling plots connected field measurements with high-resolution data. Each plot represents a cropland patch with the desired consistency.

2) Digital Photography: Digital cameras were used to measure typical vegetation (e.g., cropland or orchard) FVC according to the proposed photography guidelines [15]. These measurements formed the validation basis by providing the ground truth at the plot scale.

The FVC of each sampling plot was computed using nine images for measurement. Plot size for corn and other low-growing vegetation (below 2 m) is $10\,\mathrm{m} \times 10\,\mathrm{m}$ (Fig. 3), whereas that for fruit trees are $30\,\mathrm{m} \times 30\,\mathrm{m}$. Land surface for irrigated crops and orchards is homogeneous, such that the plot scale significantly represents an ASTER pixel scale (15 m). Cropland patches for plot location are typically larger than 2×2 ASTER pixels.

FVC was measured along two diagonals across the sampling plot, which was measured once for the overlapping section at the cross point of the two diagonals [15]. In general, nine photographs were taken. However, if the surface was homogeneous, then less than nine photographs would be sufficient. The arithmetic mean of FVC computed from the images was determined as the FVC of the plot. This sampling scheme is feasible for a plot in an irrigated cropland or orchard because of land surface homogeneity.

Most photographs were taken during cloudy days or evenings to ensure that they would be unaffected by shadows. However, the method for extracting FVC from photographs was not necessarily restricted by illumination [21]. A long stick equipped with a camera at the end was used to control shooting height. The camera was directed downward when corn was photographed. The footprint of the sensor at the nadir direction required a coverage that ranged from 1.5 to 2 times the total width of the row canopy [22]. The photographic approach guarantees that the field of view comprises two or more rows in one photograph. This strategy improves representativeness of *in situ* FVC for FVC estimation at the patch scale.

Given the tall trees in the orchard, a top-down direction was used to capture low vegetation underneath the tree crown, whereas a bottom-up direction was used to capture the underside of tree crown. FVC was obtained using [15]

$$\mathrm{FVC} = f_{\mathrm{up}} + (1 - f_{\mathrm{up}}) \cdot f_{\mathrm{down}} \tag{1}$$

where f_{up} and f_{down} are FVC values extracted from the photographs captured by the bottom-up and top-down modes, respectively. Equation (1) accounts for the FVCs of trees and understory vegetation viewed at the nadir direction between tree gaps.

3) FVC Extraction From Digital Images: Image edge distortion must be corrected before FVC can be further extracted. The perspective effect and image edge distortion caused a systematic error of up to 0.03 in the estimated FVC [23]. The most frequently used solution is cutting off image edges, such that the number of rows covered in the footprint sufficiently represents FVC at the patch scale (i.e., at least two rows). We mainly used the original thresholding method to extract FVC from the digital images [21]. This automatic classification method transfers images from the RGB color space to the Commission Internationale d'Eclairage LAB color space, which easily distinguishes green vegetation from the background. Green vegetation and nonvegetation were separated through histogram clustering, which supposes that green vegetation and the background distribution of greenness in the color space are Gaussian. The FVC of a single photograph was then computed. The original thresholding method is automatic and highly accurate. Zhao *et al*. [23] evaluated the accuracy of estimated FVC through various environmental conditions and classification methods. They compared the original thresholding method [21], which employs simulated images, with supervised classification and concluded that both methods produce similar results [23]. However, the perspective effect resulted in an error of less than 5%, which can be eliminated by cutting the edges of digital images.

The original thresholding method used in this study underestimated FVC when the photograph features deep shadows. A new thresholding method [24] was adopted by introducing a histogram equalization algorithm to preprocess images. The original thresholding method was then applied to calculate FVC after the images were enhanced. The improved classification method aims to reduce field measurement systematic errors.

The differences between the results of the two methods are plotted in Fig. 4. The estimated FVC values differed by as much as 0.2 between the two data sets as corn reached FVC maximum. By contrast, FVC values differed slightly during the early and late corn growth stages because deep shadows dramatically increased as corn grew tall and leaves became dense. The results of the supervised classification supported the feasibility of the improved method [24].

C. Remote Sensing Imagery

1) ASTER and CASI Images: ASTER L1B images were acquired from May 30 to September 14, 2012. This period is consistent with that of the ground experiment. The images had a spatial resolution of 15 m and a frequency of 15 days.

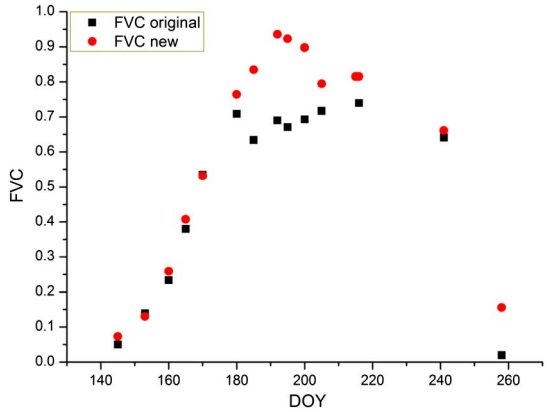

Fig. 4. Comparison between the FVC series calculated with the original thresholding method [21] and that with the new thresholding method [24] at a cropland plot. The black points represent field-measured FVC derived from the original thresholding method, whereas the red points represent the result derived from the shadow-resistant method.

Data observed by the CASI sensor [25] were collected on June 29 and July 7, 2012. This procedure obtained visible, near-infrared, and shortwave infrared airborne remote sensing data over a $30\ \mathrm{km} \times 30\ \mathrm{km}$ core observation area in the middle reaches of the Heihe River. Relative aircraft height was 2000 m (3500 m above sea level). The CASI sensor had a wavelength that ranged from 380 to 1050 nm and a spatial resolution of 1 m.

ASTER and CASI radiance images were processed through radiometric calibration, atmospheric correction, and geometric correction using synchronous measurements. ASTER and CASI projections were transformed into GEOV1 projections. Digital sounders and sun spectrophotometers detected atmospheric parameters (e.g., air temperature profiles, humidity profiles, and aerosol properties). MODIS aerosol products, as well as solar zenith angle and azimuth angle data, were also required for atmospheric correction. ASTER and CASI surface reflectance products were obtained after data processing to generate high-resolution FVC reference maps.

2) GEOV1 FVC Product: The GEOV1 FVC product (http://land.copernicus.eu/global/products/FCover) derived from SPOT/VEGETATION data from 1999 to the present was generated based on the improved CYCLOPES FVC product. The CYCLOPES project used a biophysical algorithm to generate FVC data from VEGETATION observations. This algorithm computes products at 10-day intervals and is based on neural network inversion over the $\mathrm{SAIL} + \mathrm{PROSPECT}$ radiative transfer model [16], [26]. The Validation Report of Land Surface Analysis Vegetation Products (2008) revealed that FVC values from CYCLOPES are higher than those from SEVIRI by approximately 0.15. Fillol *et al.* [18] noted that FVC products derived from CYCLOPES data are lower than those generated from high-resolution SPOT data. Camacho-de Coca *et al.* [27] observed that CYCLOPES FVC products are underestimated because of signal saturation. GEOV1 was generated by scaling CYCLOPES FVC with a constant derived from field measurements to overcome the underestimation problem [17].

The main data applied to the validation process are summarized in Table I.

TABLE I
REMOTE SENSING AND FIELD-MEASURED DATA USED FOR VALIDATION

Data type	Acquisition date	Spatial resolution (m)
GEOV1 FVC	05/24 to 09/13, 10-day interval	1000
ASTER L1B radiance	05/30, 06/15, 06/24, 07/10, 08/02, 08/11, 08/18, 08/27, 09/03, 09/12	15
CASI airborne radiance	06/29, 07/07	1
Ground-based measurements	05/30 to 09/12	–

GEOV1 FVC products were acquired from May 24 to September 23, 2012. CASI data were acquired twice and ASTER data had a temporal resolution of approximately 15 days, which do not coincide with GEOV1 generations. GEOV1 FVC was temporally interpolated during the dates of ASTER and CASI data because GEOV1 products reflect high-frequency measurements (Table I) and spatial homogeneity in the study area. Spatial matching between GEOV1 data and ASTER or CASI images was accurately performed according to distinct oasis and desert boundaries.

Reference FVC data were calculated at a high resolution to verify the coarse-resolution FVC product.

III. UPSCALING FROM FIELD MEASUREMENTS TO COARSE-RESOLUTION FVC

A. Estimating High-Resolution FVC

Data from sensors with high spatial resolution are readily available but field measurements are still necessary to assess the uncertainty of satellite products. High-resolution data are typically combined with field-measured samples to produce a high-resolution FVC map and aggregate this map at a coarse resolution.

First, we corrected high-resolution radiance data (ASTER L1B radiance) using the second simulation of a satellite signal in the solar spectrum [28] to calculate surface reflectance and normalized difference vegetation index (NDVI). Second, we employed an empirical transfer function to convert NDVI into FVC. Linear and nonlinear regressions frequently reveal good agreement between NDVI and FVC [29], [30]. Therefore, we chose an equation that combines linear and nonlinear conditions as follows:

$$\mathrm{FVC} = (a \cdot \mathrm{NDVI} + b)^k \tag{2}$$

where a, b, and k are the conversion coefficients from NDVI to FVC. The coefficient values are dependent on land type and growth date. k indicates the linearity of FVC to NDVI, where $k = 1$ corresponds to a linear form, whereas $k \neq 1$ corresponds to a nonlinear form.

We employed ground-based FVC data extracted from field-shot digital photographs and ASTER NDVI data to develop a nonlinear relationship, as shown in (2). *In situ* data were temporally interpolated at ASTER dates. The interpolation results were reasonable even during rapid vegetation growth because of the short interval of ground measurements.

TABLE II
STATISTICAL VALUES OF ASTER FVC

Date	**05/30**	**06/15**	**06/24**	**07/10**	**08/02**
Mean	0.137	0.370	0.531	0.783	0.712
Std. Dev.	0.156	0.089	0.139	0.204	0.229
R^2	0.919	0.758	0.702	0.779	0.837
RMSE	0.060	0.126	0.103	0.101	0.108
Date	**08/11**	**08/18**	**08/27**	**09/03**	**09/12**
Mean	0.671	0.615	0.620	0.406	0.120
Std. Dev.	0.226	0.212	0.162	0.148	0.088
R^2	0.830	0.862	0.792	0.636	0.371
RMSE	0.100	0.095	0.083	0.108	0.062

Averages and standard deviations were obtained from ASTER FVC images over the study area at a resolution of 15 m. R^2 and *RMSE* are derived from ASTER-fitted FVC and field-measured FVC.

Dynamic coefficient ranges were constrained in the regression calculations. FVC expansion is expressed as follows:

$$\begin{aligned} \mathrm{FVC} &= \left(\frac{\mathrm{NDVI}-\mathrm{NDVI}_{\min}}{\mathrm{NDVI}_{\max}-\mathrm{NDVI}_{\min}}\right)^k \\ &= \left[\frac{\mathrm{NDVI}}{\mathrm{NDVI}_{\max}-\mathrm{NDVI}_{\min}}+\left(-\frac{\mathrm{NDVI}_{\min}}{\mathrm{NDVI}_{\max}-\mathrm{NDVI}_{\min}}\right)\right]^k \end{aligned} \tag{3}$$

where $\mathrm{NDVI}_{\max}$ and $\mathrm{NDVI}_{\min}$ are the NDVIs of a fully covered vegetation area and bare soil, respectively. $a = \frac{1}{\mathrm{NDVI}_{\max}-\mathrm{NDVI}_{\min}}$, $b = -\frac{\mathrm{NDVI}_{\min}}{\mathrm{NDVI}_{\max}-\mathrm{NDVI}_{\min}}$.

The boundaries of a and b were determined from the empirical estimations of $\mathrm{NDVI}_{\max}$ and $\mathrm{NDVI}_{\min}$. The regression coefficients were used to generate FVC from ASTER and CASI NDVI data.

B. Estimating Coarse-Resolution FVC

GEOV1 FVC products were geometrically registered and temporally interpolated to compare with aggregated FVC from ASTER and CASI data. The preprocessing operations were acceptable because GEOV1 data exhibited a smooth temporal shape and homogeneity. To aggregate high-resolution reference maps, the difference among the point spread functions of the products should be considered during validation [9], [31]. However, this issue is complicated and has rarely been addressed. The mean values of surrounding pixels (e.g., a 3×3 pixel window) are recommended and applied for direct validation and intercomparison [11], [31]–[33]. Homogeneous $3\ \mathrm{km} \times 3\ \mathrm{km}$ areas are limited, and thus, using 3×3 pixels may introduce uncertainties [34]. Reference maps at a coarse resolution were computed by aggregating ASTER and CASI reference maps. GEOV1 and reference FVC were then compared pixel by pixel.

IV. RESULTS AND DISCUSSION

Table II lists the averages and standard deviations of ASTER FVC over 10 acquisition dates. Mean FVC varied significantly from May to September, whereas standard deviation exhibited the same trend and reached its peak at approximately 0.2 in July and August. FVC spatial variation increased during July and August because of the significant difference between vegetated land and bare surfaces (e.g., villages and roads).

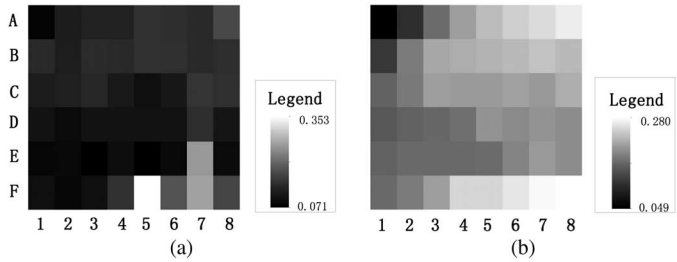

Fig. 5. Spatial distributions of aggregated (a) ASTER FVC and (b) GEOV1 FVC on May 30.

Table II also lists the squares of the sample correlation coefficients (R^2) of ASTER-fitted and field-measured FVCs over 10 ASTER image phases. ASTER FVC data were derived from ASTER NDVI data using (2) and the conversion coefficients. High-resolution FVC products exhibited the desired correlation with field-measured FVC, which increased to 0.919 on May 30. However, FVC measurements were mainly performed on corn, and FVCs measured on the same day slightly differed. R^2 varied from 0.7 to 0.9 on different dates. The fit of field measurements and high-resolution NDVI data produced a root-mean-square error (RMSE) close to 0.1 in each temporal phase. The uncertainty of fitted high-resolution FVC was reduced during upscaling when random errors were canceled out during aggregation. The validation results exhibited a low-correlation fit for FVC estimated on September 3 and an unusable fit for FVC estimated on September 12. The temporal intervals of ground measurements increased to over 10 days after August, which caused errors in temporal interpolation, particularly when vegetation grew or withered rapidly. The September 12 results were not used for further analysis.

ASTER FVC distribution aggregated to a resolution of 1 km and GEOV1 FVC presented a similar spatial pattern (Fig. 5). Corn covers most of the area, whereas the desert (black area at pixel A1 in Fig. 5) and orchards (white area at F5 and F7 in Fig. 5) are clustered. The coregistration errors of GEOV1 products and reference maps were supposed to be smaller than 1 coarse pixel because of distribution similarity.

Nine images from ASTER data were compared with GEOV1 FVC images (excluding that on September 12). The GEOV1 FVC interpolation is shown in Fig. 6. The red points represent interpolated GEOV1 FVC at ASTER acquisition dates. Reference FVCs derived from ASTER and CASI were lower than GEOV1 FVC at pixel D3.

The spatial distribution of the averages and standard deviations of the absolute difference between GEOV1 FVC and ASTER reference maps over nine dates is shown in Fig. 7. Pixels A2 and B1 were located on the boundary of the desert and oasis, wherein a high variance [Fig. 7(b)] of FVC difference and serious coregistration errors among products were observed. The average errors of GEOV1 generally increased to 0.2 compared with those of reference FVC [Fig. 7(a)].

The scatter diagrams of ASTER FVC, CASI FVC, and GEOV1 FVC over nine time phases are shown in Fig. 8. The deviation degree from the $y = x$ line was evident. When the points are far from the $y = x$ line, the difference among ASTER FVC, CASI FVC, and GEOV1 FVC is significant.

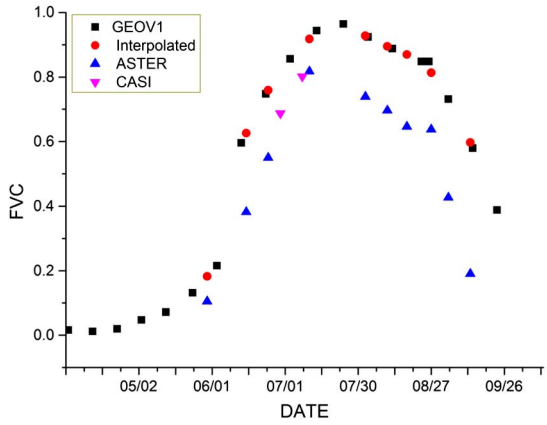

Fig. 6. Time series of GEOV1 FVC, interpolated GEOV1 FVC, aggregated ASTER FVC, and CASI FVC data of pixel D3. The black points represent the original GEOV1 FVC, whereas the red points represent the GEOV1 FVC values that were temporally interpolated on ASTER dates.

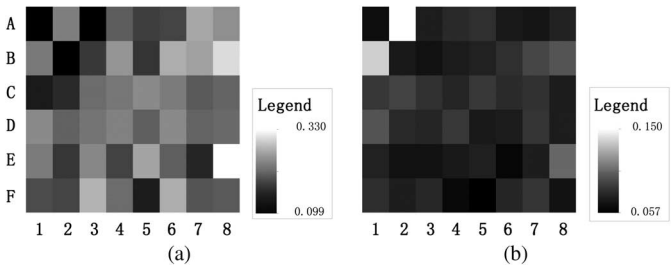

Fig. 7. GEOV1 FVC and ASTER reference FVC over nine temporal phases: (a) spatial distributions of the mean absolute difference and (b) standard deviations of the absolute difference.

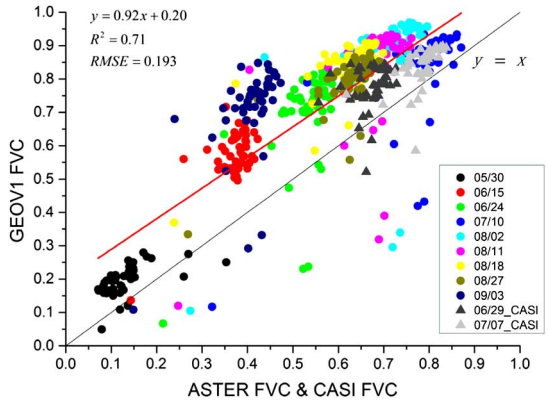

Fig. 8. Scatter plot of aggregated ASTER FVC (May 30; June 15 and 24; July 10; August 2, 11, 18, and 27; and September 3) and CASI FVC (June 29 and July 7), and their corresponding GEOV1 FVC data.

The overall RMSE of GEOV1 was 0.193, and the intercept of the regressed line was 0.20. Most points were concentrated, whereas a few points were dispersed because of the residual error in geometric rectification. The outliers in Fig. 8 correspond to the pixels near the boundary of the desert and oasis (A2 and B1), wherein spatial heterogeneity resulted in a significant product coregistration error. A single pixel in the desert (A1) corresponds to some of the lowest FVC values in Fig. 8.

The biases of GEOV1 FVC from reference FVC at ASTER and CASI acquisition dates are provided in Table III. The most unfavorable results were exhibited on September 3, i.e.,

TABLE III
AVERAGE DEVIATIONS OF GEOV1 FVC FROM REFERENCE FVC AT A RESOLUTION OF 1 KM

Date	**05/30**	**06/15**	**06/24**	**06/29**	**07/07**	**07/10**
BiasASTER	0.067	0.203	0.164	—	—	0.051
BiasCASI	—	—	—	0.104	0.055	—
Date	**08/02**	**08/11**	**08/18**	**08/27**	**09/03**	
BiasASTER	0.166	0.158	0.219	0.166	0.304	
BiasCASI	—	—	—	—	—	

BiasASTER and BiasCASI represent the average deviations of GEOV1 FVC from ASTER FVC and CASI FVC, respectively.

ASTER FVC deviated from GEOV1 FVC by over 0.3 because of the high uncertainty in the temporally interpolated FVC. FVC values were low on May 30, and a small difference between ASTER FVC and GEOV1 FVC was observed, as shown in Table III and Fig. 8. Positive biases from 0.051 to 0.219 were observed for all dates (excluding September 3).

V. UNCERTAINTY EVALUATION

The uncertainty associated with upscaling and FVC estimates at a coarse resolution should be analyzed. However, the true values of FVC are theoretically unobtainable, and each error involved in validation is difficult to analyze quantitatively (e.g., the point spread function of a product) [9]. Therefore, we focused on the systematic errors in FVC measurement and estimation although most random errors could be canceled out with upscaling [33].

FVC field measurements at the plot scale included three basic error types: 1) representativeness of pictures in a plot; 2) the measurement perspective effect; and 3) classification into vegetation and nonvegetation. Row structures affect the representativeness of the footprint of a sensor [22], [35]. Moreover, approximately 1.5–2 times the total width of a row canopy is recommended to be covered in the footprint of a sensor at the nadir direction [22]. The number of rows in the footprint is relevant to different crop stages, i.e., few rows are included at a fixed camera height when a crop grows high. However, this error is insignificant because row canopy gradually grows and becomes homogeneous, particularly after rows are closed. The camera footprint in this study covered at least two rows, as described in Section II-B. We applied a classification method after histogram equalization of the image to ensure equal misclassification probabilities of vegetation and soil [21]. Thus, the classification errors were relatively random after the algorithm was improved to be shadow-resistant [24]. The photography method overestimated FVC by up to 0.03 because of the perspective effect and camera field-of-view with a shooting height of approximately 2–3 m [23].

The sampling strategy, transfer function, and aggregation of high-resolution FVC caused upscaling error. The sampling strategy (i.e., MSN) was expected to generate sampling positions according to spatial autocorrelation and stratification. The fit between field measurements and high-resolution NDVI data resulted in residual errors, which were slightly systematic and exhibited an RMSE close to 0.1. This fitting error can be reduced by aggregating high-resolution FVC. The upscaling of field-measured FVC to high-resolution FVC benefited from

the typical spatial scale of crop patches, which covered at least 2×2 ASTER or more CASI pixels. Therefore, the spatial coregistration error from field measurements to ASTER data, as well as possible pixel-shift errors in the projection, was mostly reduced. GEOV1 products were spatially and temporally interpolated during aggregation. However, interpolation errors were unsystematic for each temporary phase and for the entire region.

Although these errors have several sources of uncertainty, the systematic errors transferred to FVC estimates at a coarse resolution cannot account for the positive bias between GEOV1 FVC and the estimated FVC during our validation.

Zhang *et al*. [36] reported that the NDVI method overestimates FVC because of land surface heterogeneity and the nonlinear relationship between NDVI and FVC. This scaling bias is discussed in [37] and [38]. However, this phenomenon does not account for most biases observed during validation. GEOV1 FVC was generated by linearly stretching CYCLOPES FVC, which was generally underestimated. Moreover, the linear stretch introduced no scaling bias.

VI. Conclusion

FVC products obtained through coarse-resolution remote sensing in typical arid and semiarid regions were validated during crop-growing season. A multistep upscaling method was applied using field-measured FVC and high-resolution images to generate coarse-resolution FVC. The distributed FVC products from the GEOV1 project and the estimated FVC were compared; the estimated FVC was considered as reference data. Field measurements at the plot scale were carefully designed to represent the spatial scale of cropland patches. This scale is comparable with an ASTER pixel resolution. High-resolution FVC data were generated from ASTER and airborne radiances through empirical fitting functions and field measurements after calibrating and preprocessing. Coarse-resolution FVC was then obtained and compared with GEOV1 FVC.

The estimated FVC was examined step by step to ensure reliable validation. GEOV1 values were found to be overestimated FVC during our validation. The systematic error that occurred in our reference FVC at a coarse resolution was less than the biases observed between reference FVC and GEOV1 FVC. Although GEOV1 FVC is significantly correlated to ASTER FVC and CASI FVC, biases of 0.051–0.219 over 11 temporary phases in the growing season of corn were found when the two data types were compared. The overall RMSE was 0.193. The uncertainty analysis exhibited possible errors associated with geometric correction, field measurements, and upscaling. These reference data errors may be influential in a small part of the area (e.g., adjacent areas of the desert). However, the systematic error over the entire study area at a coarse resolution of 1 km cannot be explained. The biases observed during validation probably resulted from errors in executing the GEOV1 algorithm when CYCLOPES FVC was scaled with a constant to generate GEOV1 FVC.

We recommend that observations over croplands be intensified worldwide to improve validations for coarse-resolution products.

Acknowledgment

The authors would like to thank the four anonymous reviewers for their patience and suggestions that have significantly improved this article. They also like to thank all of the people who provided the measured data: S. Jia, Y. Jia, L. Geng, and W. Yu from the Cold and Arid Regions Environmental and Engineering Research Institute, Chinese Academy of Sciences; Y. Huang from Northwest Normal University; J. Zhao, Y. Chen, J. Zhao, K. Yan, Y. Wang, Z. Jiao, R. Hu, and Y. Li from Beijing Normal University. The ASTER radiance data were provided by NASA. The CASI data were provided by the Institute of Remote Sensing and Digital Earth, Chinese Academy of Sciences. The GEOV1 data were provided by the European Space Agency.

References

[1] CEOS. (2012). *The Response of the Committee on Earth Observation Satellites (CEOS) to the Global Climate Observing System Implementation Plan 2010(GCOS IP-10)* [Online]. Available: http://www.ceos.org/images/WGClimate/ceos_response_to_gcos_ip-10_24_september_2012_formatted.pdf

[2] C. Justice and C. Tucker, "Coarse resolution optical sensors," in *The SAGE Handbook of Remote Sensing*. London, U.K.: SAGE Publications Limited, 2009, pp. 139–151.

[3] A. Verger, F. Camacho-de Coca, J. García-Haro, and J. Meliá, "Direct validation of FVC, LAI and FAPAR VEGETATION/SPOT derived products using LSA SAF methodology," in *Proc. IEEE Int. Geosci. Remote Sens. Symp. (IGARSS'07)*, Barcelona, Spain, 2007, pp. 3971–3974.

[4] J. Campbell, S. Burrows, S. Gower, and W. Cohen, "Bigfoot Field Manual," NASA STI/Recon, Oak Ridge, TN, USA, Tech. Rep., 1999, vol. 2, p. 12550.

[5] W. Buermann and M. Helmlinger, "SAFARI 2000 LAI and FPAR measurements at Sua Pan, Botswana, Dry Season 2000," Oak Ridge National Laboratory Distributed Active Archive Center, Oak Ridge, TN, USA, 2005 [Online]. Available: http://daac.ornl.gov/

[6] F. Baret *et al.* "VALERI: A network of sites and a methodology for the validation of medium spatial resolution land satellite products," INRA-CSE, France, 2006 [Online]. Available: http://w3.avignon.inra.fr/valeri/documents/

[7] X. Li *et al.*, "Watershed allied telemetry experimental research," *J. Geophys. Res. Atmos.*, vol. 114, no. D22, 2009, doi: 10.1029/2008JD011590.

[8] G. Gutman and A. Ignatov, "The derivation of the green vegetation fraction from NOAA/AVHRR data for use in numerical weather prediction models," *Int. J. Remote Sens.*, vol. 19, no. 8, pp. 1533–1543, 1998.

[9] J. T. Morisette *et al.*, "Validation of global moderate-resolution LAI products: A framework proposed within the CEOS land product validation subgroup," *IEEE Trans. Geosci. Remote Sens.*, vol. 44, no. 7, pp. 1804–1817, Jul. 2006.

[10] F. J. García-Haro, F. Camacho-de Coca, and J. Meliá. (2008). *Product User Manual (PUM) of Land Surface Analysis Vegetation Parameters (FVC, LAI, FAPAR)*, Portugal [Online]. Available: http://landsaf.meteo.pt/

[11] A. Verger, F. Baret, and M. Weiss, "Performances of neural networks for deriving LAI estimates from existing CYCLOPES and MODIS products," *Remote Sens. Environ.*, vol. 112, no. 6, pp. 2789–2803, 2008.

[12] M. A. White, G. P. Asner, R. R. Nemani, J. L. Privette, and S. W. Running, "Measuring fractional cover and leaf area index in arid ecosystems: Digital camera, radiation transmittance, and laser altimetry methods," *Remote Sens. Environ.*, vol. 74, no. 1, pp. 45–57, 2000.

[13] Q. Zhou and M. Robson, "Automated rangeland vegetation cover and density estimation using ground digital images and a spectral-contextual classifier," *Int. J. Remote Sens.*, vol. 22, no. 17, pp. 3457–3470, 2001.

[14] H. Zhenqi *et al.*, "Estimation of fractional vegetation cover based on digital camera survey data and a remote sensing model," *J. Chin. Univ. Min. Technol.*, vol. 17, no. 1, pp. 116–120, 2007.

[15] G. Yan, X. Mu, and Y. Liu, "Fractional vegetation cover," in *Advanced Remote Sensing: Terrestrial Information Extraction and Applications*. New York, NY, USA: Academic Press, 2012, pp. 415–438.

[16] F. Baret *et al.*, "LAI, fAPAR and fCover CYCLOPES global products derived from VEGETATION: Part 1: Principles of the algorithm," *Remote Sens. Environ.*, vol. 110, no. 3, pp. 275–286, 2007.

[17] F. Baret *et al.*, "GEOV1: LAI and FAPAR essential climate variables and FCOVER global time series capitalizing over existing products. Part 1: Principles of development and production," *Remote Sens. Environ.*, vol. 137, pp. 299–309, 2013.
[18] E. Fillol *et al.*, "Cover fraction estimation from high resolution SPOT-HRV&HRG and medium resolution SPOT-VEGETATION sensors. Validation and comparison over South-West France," in *Proc. 2nd RAQRS Symp.*, Valencia, Spain, 2006, pp. 659–663.
[19] X. Li *et al.*, "Heihe watershed allied telemetry experimental research (HiWATER): Scientific objectives and experimental design," *Bull. Amer. Meteorol. Soc.*, vol. 94, no. 8, pp. 1145–1160, 2013, doi: 10.1175/BAMS-D-12-00154.
[20] J. F. Wang, G. Christakos, and M.-G. Hu, "Modeling spatial means of surfaces with stratified nonhomogeneity," *IEEE Trans. Geosci. Remote Sens.*, vol. 47, no. 12, pp. 4167–4174, Dec. 2009.
[21] Y. Liu, X. Mu, H. Wang, and G. Yan, "A novel method for extracting green fractional vegetation cover from digital images," *J. Veg. Sci.*, vol. 23, no. 3, pp. 406–418, 2012.
[22] H. Ren *et al.*, "Impact of sensor footprint on measurement of directional brightness temperature of row crop canopies," *Remote Sens. Environ.*, vol. 134, pp. 135–151, 2013.
[23] J. Zhao, D. Xie, X. Mu, Y. Liu, and G. Yan, "Accuracy evaluation of the ground-based fractional vegetation cover measurement by using simulated images," in *Proc. IEEE Int. Geosci. Remote Sens. Symp. (IGARSS)*, Munich, Germany, 2012, pp. 3347–3350.
[24] W. Song, X. Mu, S. Huang, G. Yan, and J. Zhou, "A shadow-resistant algorithm for extracting fractional vegetation cover from digital images and its application in HiWATER," *J. Veg. Sci.*, 2014, submitted for publication.
[25] X. Qing and W. Jianguang. (2012, Jun. 29). *HiWATER: Visible and Near-Infrared Hyperspectral Radiometer*, Institute of Remote Sensing and Digital Earth, Chinese Academy of Sciences [Online]. Available: http://westdc.westgis.ac.cn/
[26] W. Verhoef, "Light scattering by leaf layers with application to canopy reflectance modeling: The SAIL model," *Remote Sens. Environ.*, vol. 16, no. 2, pp. 125–141, 1984.
[27] F. Camacho-de Coca *et al.*, "Prototyping of FCover product over Africa based on existing CYCLOPES and JRC products for VGT4Africa," in *Proc. 2nd RAQRS Symp.*, Valencia, Spain, 2006, pp. 722–727.
[28] E. F. Vermote, D. Tanré, J. L. Deuze, M. Herman, and J.-J. Morcette, "Second simulation of the satellite signal in the solar spectrum, 6S: An overview," *IEEE Trans. Geosci. Remote Sens.*, vol. 35, no. 3, pp. 675–686, May 1997.
[29] J. Xiao and A. Moody, "A comparison of methods for estimating fractional green vegetation cover within a desert-to-upland transition zone in central New Mexico, USA," *Remote Sens. Environ.*, vol. 98, no. 2, pp. 237–250, 2005.
[30] F. Li, W. P. Kustas, J. H. Prueger, C. M. Neale, and T. J. Jackson, "Utility of remote sensing-based two-source energy balance model under low- and high-vegetation cover conditions," *J Hydrometeorol.*, vol. 6, no. 6, pp. 878–891, 2005.
[31] M. Weiss, F. Baret, S. Garrigues, and R. Lacaze, "LAI and fAPAR CYCLOPES global products derived from VEGETATION. Part 2: Validation and comparison with MODIS collection 4 products," *Remote Sens. Environ.*, vol. 110, pp. 317–331, 2007.
[32] M. Claverie *et al.*, "Validation of coarse spatial resolution LAI and FAPAR time series over cropland in southwest France," *Remote Sens. Environ.*, vol. 139, pp. 216–230, 2013.
[33] F. Camacho, J. Cernicharo, R. Lacaze, F. Baret, and M. Weiss, "GEOV1: LAI, FAPAR essential climate variables and FCOVER global time series capitalizing over existing products. Part 2: Validation and intercomparison with reference products," *Remote Sens. Environ.*, vol. 137, pp. 310–329, 2013.
[34] H. Fang, S. Wei, and S. Liang, "Validation of MODIS and CYCLOPES LAI products using global field measurement data," *Remote Sens. Environ.*, vol. 119, pp. 43–54, 2012.
[35] P. Colaizzi *et al.*, "Radiometer footprint model to estimate sunlit and shaded components for row crops," *Agron. J.*, vol. 102, pp. 942–955, 2010.
[36] X. Zhang, G. Yan, Q. Li, Z.-L. Li, and H. Wan, "Evaluating the fraction of vegetation cover based on NDVI spatial scale correction model," *Int. J. Remote Sens.*, vol. 27, no. 24, pp. 5359–5372, 2006.
[37] H. Wu and Z.-L. Li, "Scale issues in remote sensing: A review on analysis, processing and modeling," *Sensors*, vol. 9, no. 3, pp. 1768–1793, 2009.
[38] H. Wu, B.-H. Tang, and Z.-L. Li, "Impact of nonlinearity and discontinuity on the spatial scaling effects of the leaf area index retrieved from remotely sensed data," *Int. J. Remote Sens.*, vol. 34, no. 9–10, pp. 3503–3519, 2013.

Xihan Mu received the B.S. degree in computer science and technology from the College of Information Science and Technology, Beijing Normal University, Beijing, China, in 1999, and the Ph.D. degree in remote sensing from the School of Geography, Beijing Normal University, in 2009.

He was a Visiting Student at the Laboratoire des Sciences de l'Image, de l'Informatique et de la Télédétection (LSIIT), Université de Strasbourg, France, in 2007. He is currently an Assistant Scientist with the School of Geography, Beijing Normal University. His research interests include multiangular remote sensing to retrieve leaf area index, fractional vegetation cover, and land surface temperature.

Shuai Huang is currently pursuing the M.S. degree from Beijing Normal University, Beijing, China.

Her research interests focus on the retrieval and measurement of fractional vegetation cover.

Huazhong Ren received the Ph.D. degree in remote sensing from Beijing Normal University, Beijing, China, and from the Université de Strasbourg, Strasbourg, France, in 2013.

He is currently a Postdoctoral Researcher with the Institute of Remote Sensing and Geographic Information System, Peking University, Beijing, China. His research interests include the retrieval of land surface temperature/emissivity and their angular correction. He has also devoted his efforts to the spectral calibration of broadband images for airborne and spaceborne instruments.

Guangjian Yan received the Ph.D. degree from the Institute of Remote Sensing Applications, Chinese Academy of Sciences, Beijing, China, in 1999.

He is currently a Professor with Beijing Normal University, Beijing, China. He has published more than 100 papers. His research interests include multiangular and thermal infrared remote sensing.

Wanjuan Song is currently pursuing the M.S. degree from Beijing Normal University, Beijing, China.

Her research interests include fractional vegetation cover and vegetation modeling on complex surface area.

Gaiyan Ruan is currently pursuing the M.S. degree from Beijing Normal University, Beijing, China.

Her research interests include the extraction and retrieval of fractional vegetation cover in mountain areas.